

DATA REPOSITORY

APPENDIX: DATING METHODOLOGY

1. OPTICALLY STIMULATED LUMINESCENCE DATING

1.1 SAMPLING STRATEGY

The sampling strategy for optically stimulated luminescence (OSL) dating targeted the sedimentary lithofacies of rippled sands (Sr), horizontally-bedded sands (Sh) and planar-bedded sands (Sp) to maximise the potential for the grains to have been exposed to sunlight prior to sediment burial (after Thrasher et al., 2009). Coastal and quarry exposures of glaciofluvial sediments deposited when the ice was last present at each site were sampled to constrain the timing of ice retreat i.e. towards the top of each sedimentary sequence. OSL dating complements the pre-existing CN ages for Mynedd Mawr, Llŷn Peninsula, and Holyhead Mountain, Anglesey (McCarroll et al. 2010) that have been recalculated here, and also constrain the timing of ice retreat across the Llŷn Peninsula. By combining OSL and CN ages for an ice retreat across the Llŷn Peninsula, we provide robust chronology reconstructing deglaciation of the last British-Irish Ice Sheet as discussed in Small et al. (2017).

1.2 FIELD SAMPLING

Cefn Mine: Two large fans drain from the southern ends of the larger cols that breach the bedrock core to the Llŷn Peninsula at Rhoslan and Cors Geirch. The Cors Geirch fan has been interpreted as a marine (Eyles and McCabe, 1989) or lacustrine delta (McCarroll, 2005; Thomas and Chiverrell, 2007). Following the glaciolacustrine model, the Cors Geirch terraces (at +80 m above Ordnance Datum (OD) maximum) are an extensive proglacial outwash delta formed at a time when the Irish Sea Ice Stream (ISIS) margin straddled the Llŷn Peninsula discharging into a lake dammed by Snowdonian ice (Thomas and Chiverrell, 2007). At Cefn Mine (52.896 °N 4.472 °W) exposures cut into the +50 m OD terrace show low angle outwash delta fore-set sands dipping southwest and capped by delta top-set gravels (Thomas and Chiverrell, 2007). Two samples were sampled for OSL dating from depths of 3.5 m (T4CEIF02) and 12 m (T4CEIF01) below the cliff top.

Morfa Nefyn: Set immediately north of the bedrock core to the Llŷn Peninsula, 6 km of coastal exposures from Porth Dinllaen to Penrhyn Glas record a complex sequence of glacial diamictons, glaciofluvial sands, gravels and glaciolacustrine muds (referred to as Sequence A to C in Thomas and Chiverrell, 2007). Palaeocurrent directions in the glaciofluvial outwash throughout the sequence indicate flow to the SW funnelled between the ice margin and the bedrock ridge (for details see Thomas and Chiverrell, 2007). The exposures at Morfa Nefyn (52.937 °N 4.548 °W) show that above bedrock a basal Irish Sea type diamicton and overlying outwash gravels, sands and muds (Sequence

A; Thomas and Chiverrell, 2007) record the advance and retreat of the ISIS. Sequence B records an erosional contact to basal channel gravels and overlying stacked gravel bars deposited as a NE-SW sandur system. Sequence B in turn is buried by a rapid shift to upper (Sequence C; Thomas and Chiverrell, 2007) fan gravels and intercalated diamict suggestive of a minor ice readvance of the ice-margin or ice-marginal debris flows into the sandur system. An OSL sample (T4MNEF03; Fig. DR1) was taken from rippled medium-coarse sands 5 m below the top of the section and from the base of Sequence C.

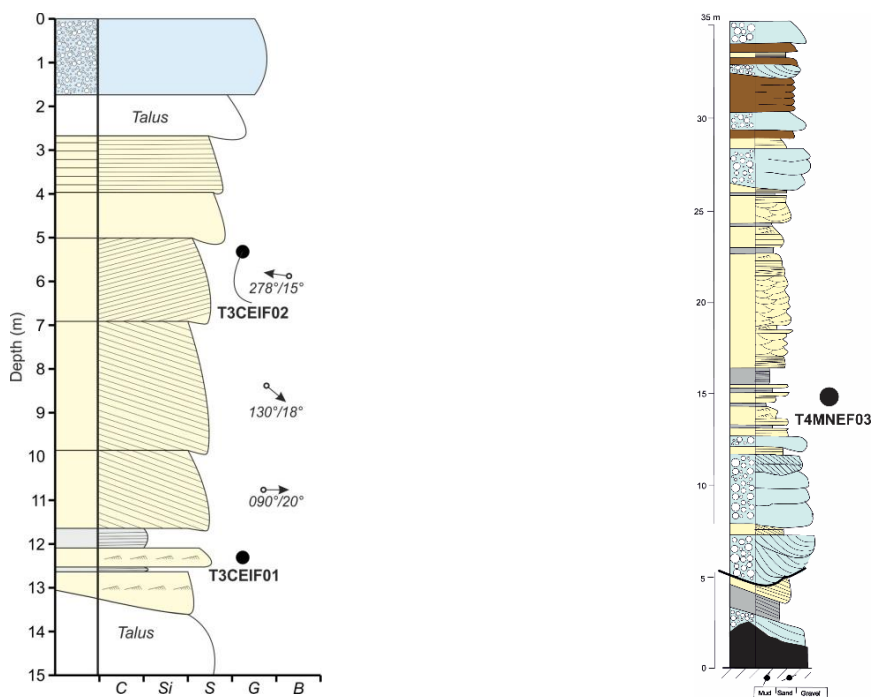


Fig. DR1. Sedimentary units sampled for samples T4CEIF01 and T4CEIF02 (left) and sample T4MNEF03 (right; Fig. 10, Thomas and Chiverrell, 2007).

Bryn-y-Eryr: Coastal exposures 1.5 km in length extending south from Aberafon to Bryn-yr-Eryr show a basal tectonised Irish Sea type diamict and associated outwash deposits with an erosional upper surface that crops out in the south (Fig. DR2). Set above this are five discrete sedimentary sequences that form an offlapping and transgressive succession to the south. Each sequence comprises a diamict passing southwards away from the ice margin into ice-proximal outwash gravel and then more ice-distal outwash sands. The sequences are bounded above and below by unconformities and offlap in a down-ice direction (for detail see Thomas and Chiverrell, 2007). The sequence is interpreted as a complex five stage and transgressive 1 km readvance of the ISIS involving phased forward movement, with each phase extending further down-ice. The diamict within this stage typically coincides with a pronounced moraine ridge form in the geomorphology. Two OSL samples were taken from back-bar planar cross-stratified sand units in a dominantly gravel sediment sequence (Fig. DR2) similar in character to the ice proximal facies assemblage of Thomas et al. (1985).

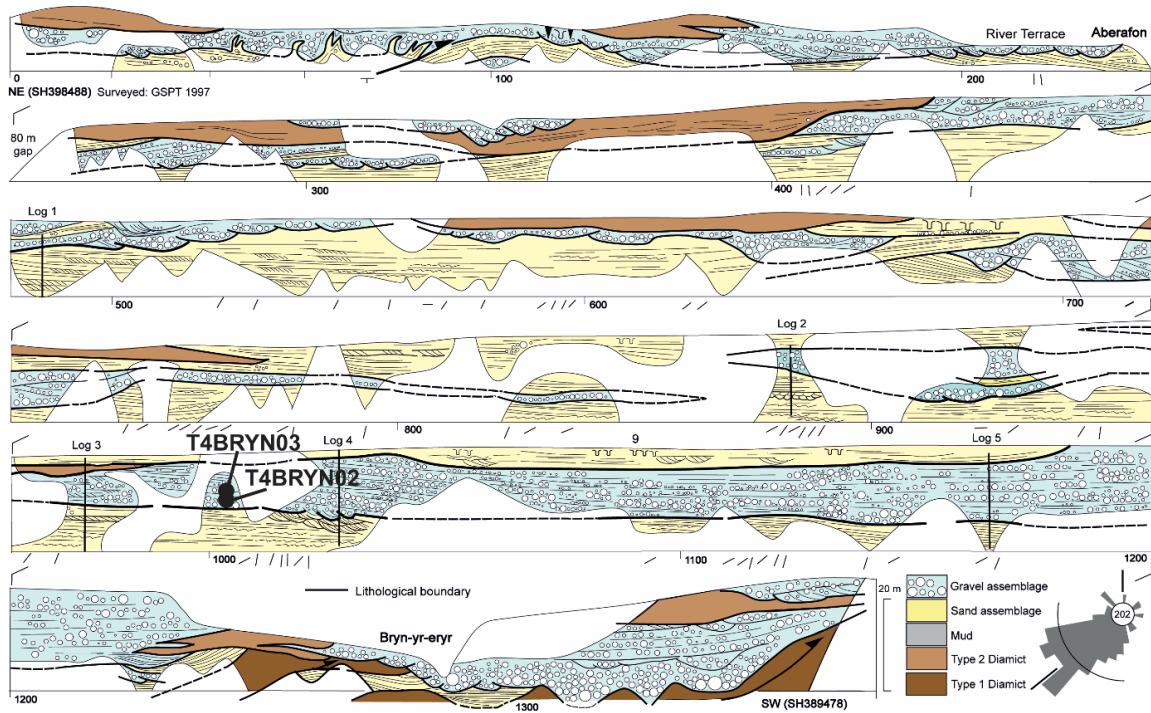


Fig. DR2. Sedimentary units sampled for samples T4BRYN02 and T4BRYN03 (Fig. 13; Thomas and Chiverrell, 2007).

Aberdesach: The pronounced ridge form at Aberdesach exhibits an asymmetric shape with steeper ice-contact and shallower down-ice slopes, with > 650 m of coastal exposure showing a complex glaciotectionised stratigraphy (Fig. DR3; Thomas and Chiverrell, 2007). The exposures show evidence for ice advance (Sequence A; Thomas and Chiverrell, 2007), retreat and subsequent readvance (Sequence B; Thomas and Chiverrell, 2007), with two separate closely-related advances of the ice margin. The readvance was responsible for the tectonic deformation of the basal Sequence A. The sample (T4ADES01) was taken from horizontally-stratified medium to coarse sands 0.1 m thick within Sequence A (Fig. DR3; Thomas and Chiverrell, 2007).

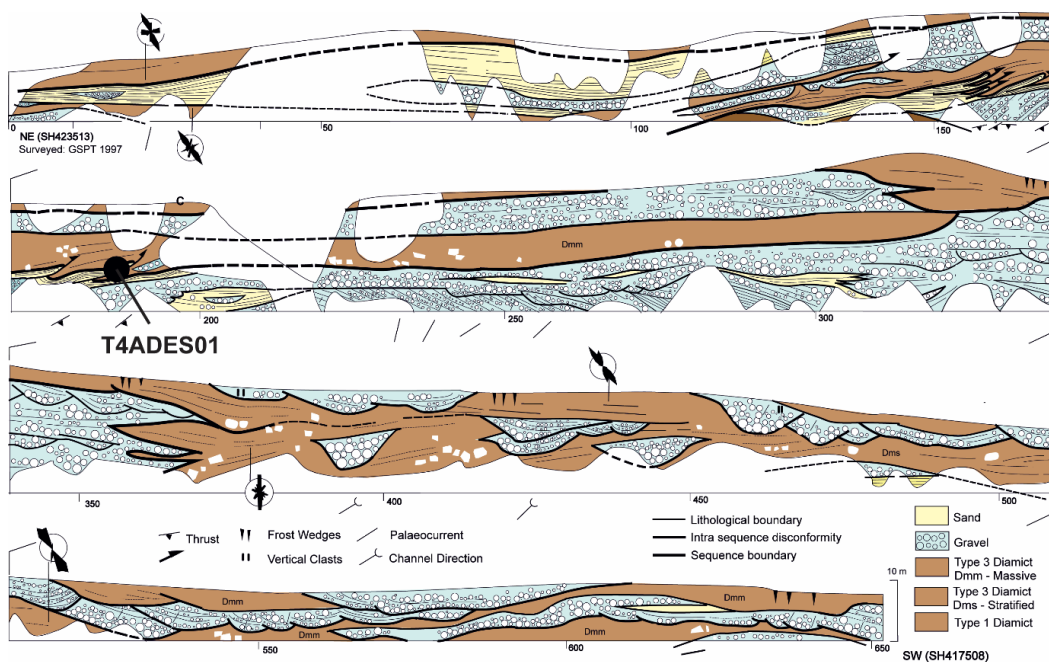


Fig. DR3. Sedimentary units sampled for sample T4ADES01 (Fig. 17; Thomas and Chiverrell, 2007).

Aberogwen: Coastal exposures at Aberogwen (Edge et al., 1990) show a basal glacial diamict of Welsh provenance overlain by a 2 m thick sequence of laminated sands, silts and clays lapping-off west to east from a diamict high. These horizontal laminated glaciolacustrine deposits lie under and interdigitate with a unit of east to west dipping (30 °) gravel and sand foresets. This lacustrine and deltaic ice-marginal sequence is capped by glacial diamict of Irish Sea affinity. Two OSL samples were taken, targeting a 0.15 m thick unit (3.5 m depth) of horizontally stratified medium to coarse sand (Sh) above the basal diamict (T4ABER01) and a 0.06 m thick unit (1.7 m depth) of horizontally stratified medium-to-coarse ice-proximal bottom-set sands (T4ABER03).



Fig. DR4. Coastal exposure of sediments at Aberogwen which were sampled for OSL dating (samples T4ABER01 and T4ABER03). Note that the exposure (A) is ca. 3.5 m high.

1.3. ENVIRONMENTAL DOSIMETRY

External beta dose-rates were determined from U, Th, K and Rb concentrations from milled and homogenised bulk sediment samples using inductively coupled plasma mass spectrometry (ICP-MS) and atomic emission spectroscopy (ICP-AES). External gamma dose-rates were determined using in-situ gamma spectrometry. The beta dose-rates (Table DR1) were calculated using the conversion factors of Guerin et al. (2011) and beta dose-rate attenuation factors of Guerin et al. (2012). External beta dose-rates were also determined for each sample using a Risø GM-25-5 beta counter and were within measurement uncertainties of the beta dose-rates determined using the geochemical analyses. Water contents were estimated considering the field and saturated water contents, and the environmental history for each sample. Cosmic dose-rates were calculated after Prescott and Hutton (1994).

Table DR1. Environmental dose-rates to grains of quartz, determined using ICP-MS and ICP-AES analysis and field gamma spectrometry. The chemical concentrations are presented to the appropriate decimal places according to the associated detection limit. The grain size for all samples was 212 – 250 μm . The water contents are expressed as a percentage of the mass of dry sediment. Dose-rates were calculated using the Dose Rate and Age Calculator (DRAC; Durcan et al., 2015).

Sample	Depth (m)	Water content (%)	K (%)	Rb (ppm)	U (ppm)	Th (ppm)	Beta dose-rate (Gy/ka)	Gamma dose-rate (Gy/ka)	Cosmic dose-rate (Gy/ka)	Total dose-rate (Gy/ka)
T4CEIF01	12.0	20 \pm 5	1.1 \pm 0.1	38.4 \pm 3.8	1.27 \pm 0.13	4.5 \pm 0.5	0.83 \pm 0.08	0.48 \pm 0.03	0.05 \pm 0.01	1.39 \pm 0.08
T4CEIF02	3.5	17 \pm 5	0.9 \pm 0.1	34.5 \pm 3.5	0.84 \pm 0.08	3.3 \pm 0.3	0.68 \pm 0.07	0.37 \pm 0.03	0.13 \pm 0.01	1.19 \pm 0.07
T4MNEF03	5.0	17 \pm 5	0.9 \pm 0.1	35.0 \pm 3.5	0.86 \pm 0.09	3.2 \pm 0.3	0.68 \pm 0.07	0.39 \pm 0.03	0.11 \pm 0.01	1.19 \pm 0.07
T4BRYN02	12.0	17 \pm 5	1.5 \pm 0.2	58.1 \pm 5.8	1.25 \pm 0.13	5.8 \pm 0.6	1.12 \pm 0.11	0.72 \pm 0.05	0.05 \pm 0.01	1.92 \pm 0.12
T4BRYN03	12.0	17 \pm 5	1.8 \pm 0.2	77.6 \pm 7.8	1.63 \pm 0.16	8.5 \pm 0.9	1.38 \pm 0.13	0.81 \pm 0.05	0.09 \pm 0.01	2.28 \pm 0.14
T4ADES01	7.0	17 \pm 5	1.5 \pm 0.2	60.9 \pm 6.1	1.42 \pm 0.14	6.4 \pm 0.6	1.15 \pm 0.11	0.96 \pm 0.07	0.09 \pm 0.01	2.22 \pm 0.13
T4ABER01	3.5	23 \pm 5	1.8 \pm 0.2	80.9 \pm 8.1	2.10 \pm 0.21	8.5 \pm 0.9	1.34 \pm 0.12	0.84 \pm 0.06	0.13 \pm 0.01	2.35 \pm 0.14
T4ABER03	1.7	23 \pm 5	1.8 \pm 0.2	93.0 \pm 9.3	2.58 \pm 0.26	11.5 \pm 1.2	1.43 \pm 0.13	0.91 \pm 0.06	0.16 \pm 0.02	2.55 \pm 0.14

1.4. EQUIVALENT DOSES

Grains of quartz used to determine equivalent doses (D_e) were isolated by treating each sample with a 10 % v/v dilution of 37 % HCl and with 20 v/v of H_2O_2 to remove carbonates and organics, respectively. Dry sieving then isolated the 212 – 250 μm diameter grains for all samples. Density separation using sodium polytungstate then provided the 2.62 – 2.70 g cm^{-3} (quartz-dominated) fractions, which were etched for 1 h in 40 % hydrofluoric acid (HF) to remove the outer portion of the quartz grains that was affected by alpha irradiation and any contaminating feldspar. Grains were then washed in a 10 % solution of HCl to remove any fluorides that may have been produced during the HF etch. Finally, grains of quartz were mounted on a 9.8 mm diameter aluminium single-grain disc for analysis, which contained a 10 by 10 grid of 300 μm diameter holes.

All luminescence measurements were performed using a Risø TL/OSL DA-15 automated single-grain system equipped with a $^{90}\text{Sr}/^{90}\text{Y}$ beta source (Bøtter-Jensen et al., 2003). Optical stimulation was performed for 1 s using a green laser at 125 $^\circ\text{C}$ and the OSL signal was detected through a 2.5 mm thick U-340 filter and convex quartz lens placed in front of the photomultiplier tube. The first 0.1 s and final 0.2 s of stimulation were summed to calculate the initial and background OSL signals, respectively (e.g. Fig. DR5a). A preheat plateau test performed on 5 mm aliquots of sample T4CEIF01 was used to determine the preheat temperature (200 $^\circ\text{C}$ for 10 s) applied throughout the single aliquot regenerative dose (SAR) protocol (Murray and Wintle, 2000). A cutheat of 160 $^\circ\text{C}$ and test dose of ~ 10 Gy were also used for analyses. An example of a typical dose-response curve is shown in Fig. DR5b. The distribution of OSL signal intensity for single grains of quartz was similar for all of the samples (Fig. DR5c). Dose-recovery experiments were performed on all of the samples where the OSL signals were bleached using blue light emitting diodes (LEDs). The results confirmed that the SAR protocol used for analysis was appropriate as each sample could recover the given dose within ± 10 % and the overdispersion determined from the single-grain D_e distributions quantified the amount of scatter caused by intrinsic sources of uncertainty (Fig. DR6).

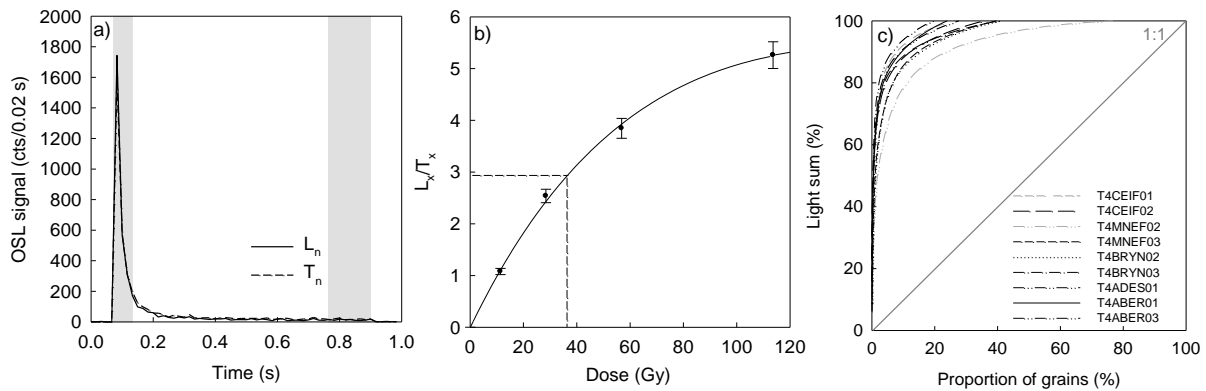


Fig. DR5. Examples of typical decay curves (a) and a dose-response curve (b) for a single grain from sample T4CEIF01. The grey shading represents the summation intervals used. The distribution of the signal intensity emitted by the quartz grains in this study (c).

The grains were accepted after applying the following screening criteria and accounting for the associated uncertainties: (1) whether the test dose response was greater than three sigma above the background, (2) whether the test dose uncertainty was less than 20 %, (3) whether the recycling and OSL-IR depletion ratios were within the range of ratios 0.8 to 1.2, (4) whether recuperation was less than 5 % of the response from the largest regenerative dose and (5) whether the single-grain D_e values were not from a population of very low doses that were identified by the finite mixture model (FMM) to be inconsistent with the geological context of the sample (i.e. < 1 ka). Grains were only removed by the final screening criterion from the datasets for samples T4BRYN02 and T4BRYN03, accounting for only 2 % ($n = 1$ grain) and 3 % ($n = 2$ grains) of the grains passing all other criteria, respectively. D_e values were calculated from all grains passing all the screening criteria (Fig. DR7; Table DR2) and incorporated an uncertainty from instrument reproducibility of 2.5 % (Thomsen et al., 2005).

Table DR2. Results from OSL dating of the samples from the Llŷn Peninsula, including the total number of grains analysed and the number of grains (n) that passed the screening criteria. The overdispersion (OD) from intrinsic sources of uncertainty was determined from dose-recovery (DR) experiments and combined in quadrature with OD from extrinsic sources (20 %). The overdispersion values determined from intrinsic and extrinsic sources were rounded to the nearest 0.05 for consistency and used to determine the respective σ_b values for the MAM (three-parameter model).

Sample	Total grains	n	CAM D_e (Gy)	CAM age (ka)	Natural (%)	DR (%)	σ_b	MAM D_e (Gy)	MAM age (ka)
T4CEIF01	4,000	54	-	-	72	32	0.40	30.4 ± 5.8	21.9 ± 4.4
T4CEIF02	3,900	67	-	-	63	23	0.30	21.4 ± 3.4	18.0 ± 3.0
T4MNEF03	2,000	44	-	-	66	19	0.25	25.8 ± 4.1	21.8 ± 3.7
T4BRYN02	2,400	56	37.8 ± 2.3	19.7 ± 1.7	39	27	-	-	-
T4BRYN03	2,900	69	43.7 ± 2.5	19.2 ± 1.6	41	34	-	-	-
T4ADES01	5,900	77	-	-	48	21	0.30	41.9 ± 6.5	18.9 ± 3.1
T4ABER01	2,400	33	42.5 ± 3.0	18.1 ± 1.6	34	0	-	-	-
T4ABER03	4,800	46	51.5 ± 4.0	20.2 ± 1.9	47	19	-	-	-

1.5. DETERMINING OSL AGES

Symmetrical D_e distributions were determined for four out of the eight samples (Fig. DR7; T4BRYN02, T4BRYN03, T4ABER01, T4ABER03) and suggest that these grains were homogeneously bleached prior to burial; thus the central age model (CAM; Galbraith et al., 1999) was used to determine ages. The D_e distributions determined for the four remaining samples (Fig. DR7; T4CEIF01, T4CEIF02, T4MNEF02, T4MNEF03, T4ADES01) were characterised by asymmetrical D_e distributions typical of sediments that were heterogeneously bleached prior to burial. The minimum age model (MAM; Galbraith and Laslett, 1993; Galbraith et al., 1999) was therefore used to determine ages for these samples.

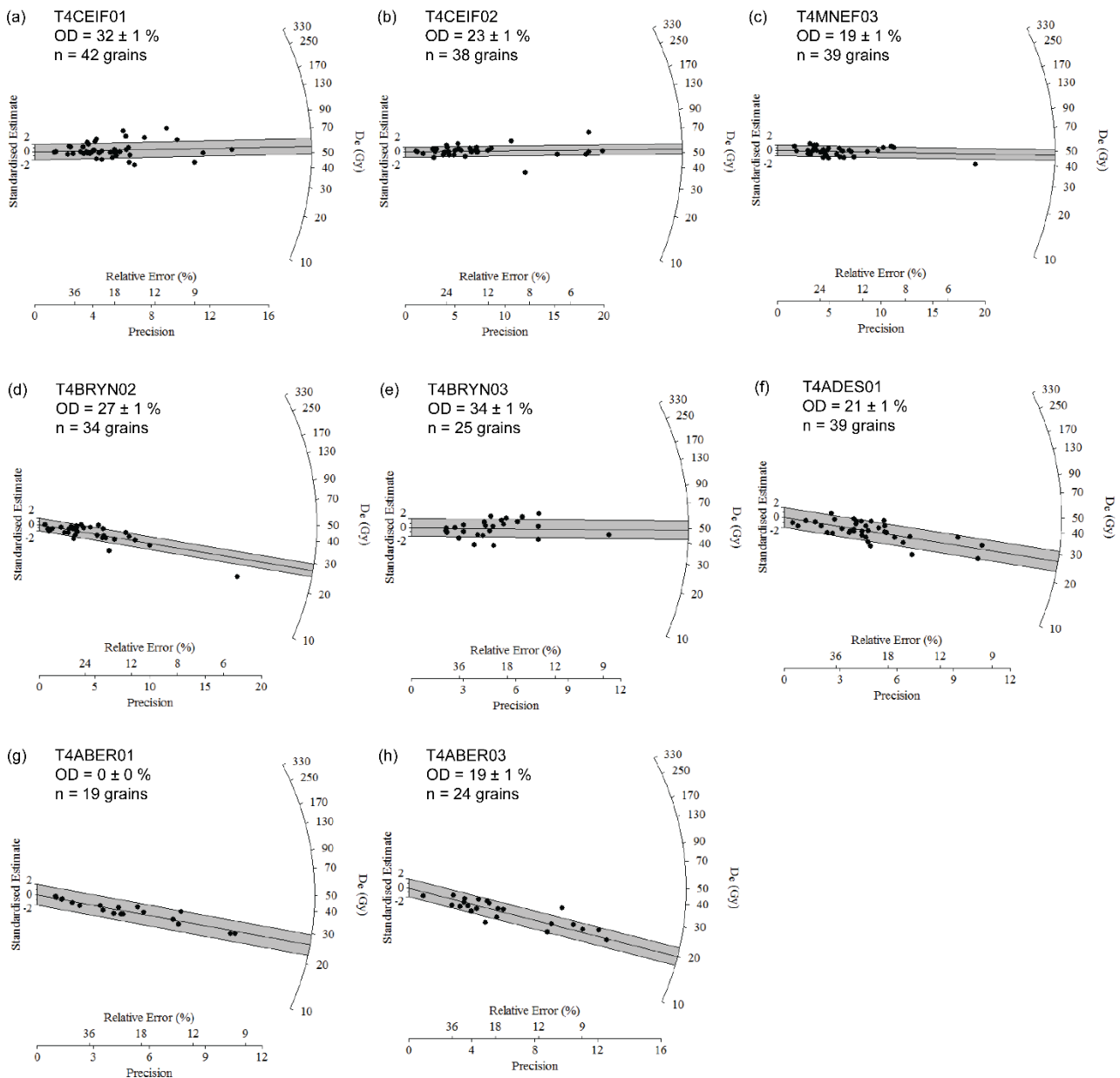


Fig. DR6. Radial plots showing the single-grain D_e values determined from the dose-recovery experiments. The overdispersion of each dataset is shown in this figure and listed in Table DR2.

The amount of scatter in the well bleached part of a heterogeneously-bleached D_e distribution (or σ_b) needs to be quantified to determine accurate ages using the MAM. Scatter in a single-grain D_e distribution determined for a well-bleached sample can arise from intrinsic (i.e. luminescence characteristics and instrument reproducibility) and/or extrinsic (i.e. external microdosimetry) sources of uncertainty (e.g. Thomsen et al., 2005). The overdispersion from intrinsic sources of uncertainty has been quantified for each sample using dose-recovery experiments (Fig. DR6). Additional overdispersion was then added to this in quadrature to account for scatter arising from external microdosimetry (~20 %) and determine σ_b , which was rounded to the nearest 5 % for consistency. The D_e values were divided by the environmental dose-rates to determine an age for each sample. The OSL ages determined for each sample from the LIÿn Peninsula are shown in Table DR2.

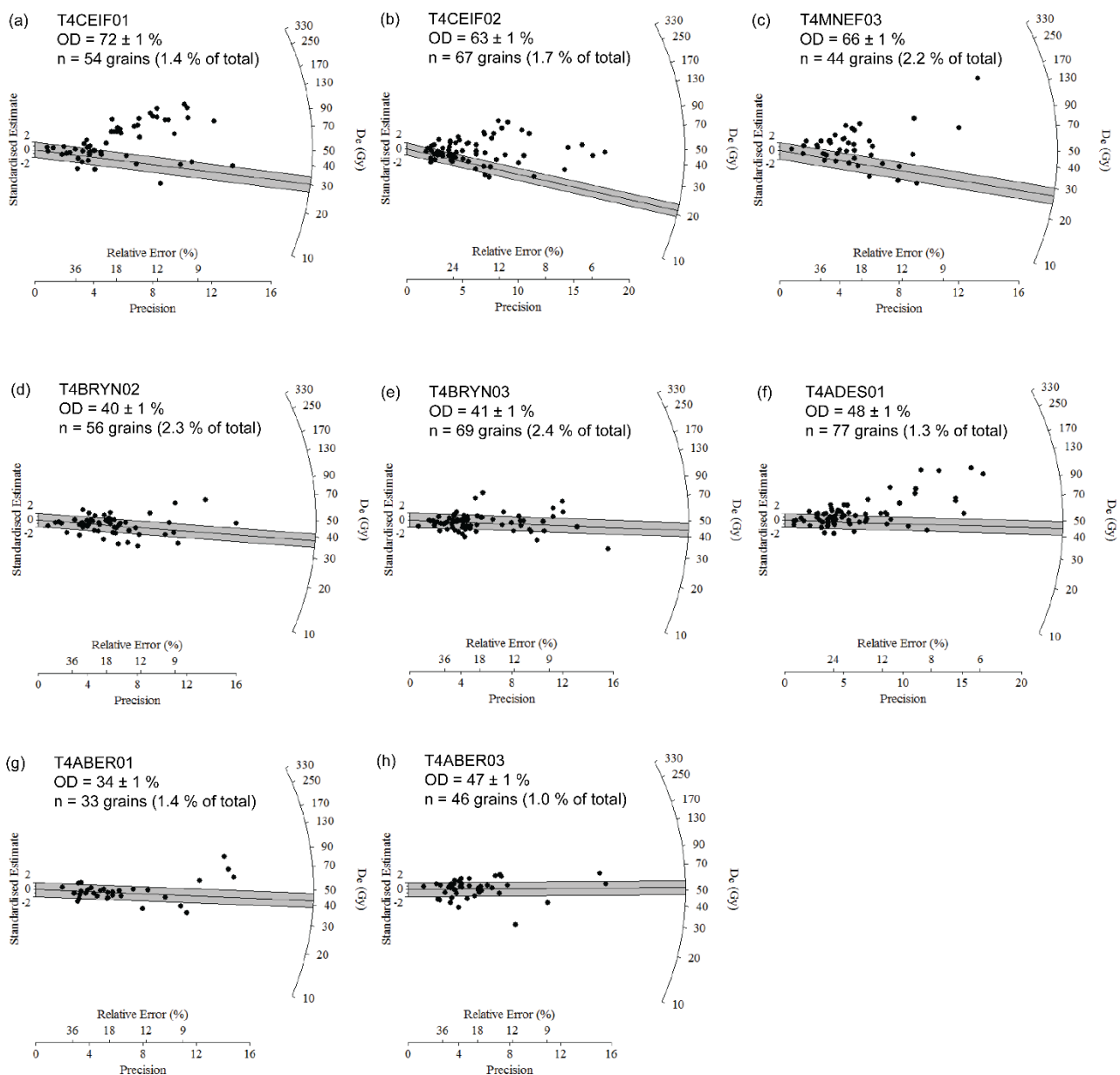


Fig. DR7. Radial plots showing the single-grain D_e values determined from quartz.

2. RE-CALCULATING CN AGES

The ^{10}Be exposure ages from McCarroll et al. (2010) have been re-calculated here using a local production rate, the Loch Lomond production rate (LLPR; Fabel et al., 2012). This yields a reference sea-level high latitude production rate of 4.00 ± 0.17 atoms g^{-1} quartz for the Lm scaling scheme. Ages were re-calculated using the CRONUS-Earth online calculator (Table DR3; Balco et al., 2008). Exposure ages presented are based on the time-dependent Lm scaling (Lal, 1991; Stone, 2000) and assuming an erosion rate of 1 mm ka^{-1} . Two CN ages obtained for ice-scoured and striated quartzite outcrops at Mynedd Mawr at ca. +130 m O.D. near the western end of the Llŷn Peninsula constrain the pull back of ice from the bedrock core of the peninsula (Chiverrell et al., 2013; McCarroll et al., 2010). Further north glacially scoured quartzite bedrock at 190 – 205 m OD in W Anglesey (Holyhead Mountain) has yielded five CN ages (Chiverrell et al., 2013; McCarroll et al., 2010). Although the exposure ages for the bedrock samples at Mynedd Mawr on the Llŷn Peninsula were in agreement with one another, the likelihood of nuclide inheritance in bedrock samples could not be ruled out (McCarroll et al., 2010). Thus, the ages represent a maximum constraint on deglaciation of this site.

Table DR3. CN ages from McCarroll et al. (2010) re-calculated using the LLPR. The calculations were performed using the CRONUS-Earth online calculator developmental version; wrapper script 2.3, Main calculator 2.1, constants 2.3, muons 1.1. The highlighted sample (*) was identified as an outlier in McCarroll et al. (2010) with the remaining four samples yielding a reduced chi-square of 1.09.

	Sample	McCarroll et al. (2010) ages	Analytical uncert	Uncert.	LLPR ages	Uncert.
Holyhead Mountain, Anglesey	HM-01*	20.48	0.78	2.14	23.4	1.3
	HM-2.1	17.94	0.60	1.85	20.4	1.1
	HM-2.2	18.88	0.84	2.01	21.5	1.3
	HM-03	18.62	0.71	1.94	21.2	1.2
	HM-04	17.71	0.48	1.80	20.2	1.0
Mynedd Mawr, Llŷn Peninsula	MM-01	22.55	0.65	2.30	26.0	1.4
	MM-02	21.27	0.78	2.21	24.3	1.4

3. BAYESIAN MODELLING

The ages presented here are considered as independent measurements (Bronk Ramsey, 1995), and exist within a spatial framework that allows the sequence of events (geomorphological features or sedimentary units) to be determined independently of the chronological measurements (Bronk Ramsey, 2008; Bronk Ramsey, 2009a; Buck et al., 1996; Chiverrell et al., 2013). This prior model (in Bayesian terminology), a relative order of events, comprises the series of independent age measurements and provides a basis for using Bayesian age modelling (Bronk Ramsey, 2009a; Buck et al., 1996). The Bayesian approach has the advantages of robust handling of outliers (Bronk Ramsey, 2009a, b; Buck et al., 1996) and the modelling can reduce age uncertainties (Chiverrell et al., 2013). In constraining glacial chronologies the prior model consists of a sequence of locations arranged in the order by which they deglaciated discerned from geomorphology and stratigraphy (Thomas and Chiverrell 2007). The Bayesian approach compares the overlap between the likelihood probability distribution and the modelled posterior probability distribution (Bronk Ramsey, 2009a) to identify outliers. The Bayesian modelling was undertaken in OxCal 4.2 (Bronk Ramsey, 2013;

http://c14.arch.ox.ac.uk) using a uniform phase Sequence model and uses a Markov chain Monte Carlo (MCMC) sampling to build up a distribution of possible solutions generating a probability called a posterior density estimate, the product of both the prior model and likelihood probabilities, for each sample. The model was set up as an outlier model (Bronk Ramsey, 2009a) to assess for outliers in time (t), which is appropriate given the integration of OSL and CN dating techniques, and using a student's t-distribution to define how the outliers are distributed and a scale of $10 - 10^4$ years (Bronk Ramsey, 2009a). All measurements were assigned a prior probability of 0.05 of being an outlier, with OSL age T4CEIF02 and CN determinations MM1 and HM-1 plotting as significant outliers in initial model runs and then assigned an outlier prior probability of 0.75. The Sequence models divide into a series of Phases, each representing the geochronology for specific sites grouping dating information that shares common relationships with other items in the model. Phases (grouped information) and individual ages are separated by the Boundary command which delimit the period of each Phase and generates the modelled age estimates used constrain the movement of the ISIS margin across the Llŷn Peninsula. The model code is shown in Data Repository Section 5. The approach produced a conformable age model for the ice marginal retreat sequence (Figure DR8) with an overall model agreement index >87.7 % exceeding the >60 % threshold advocated by Bronk Ramsey (2009a).

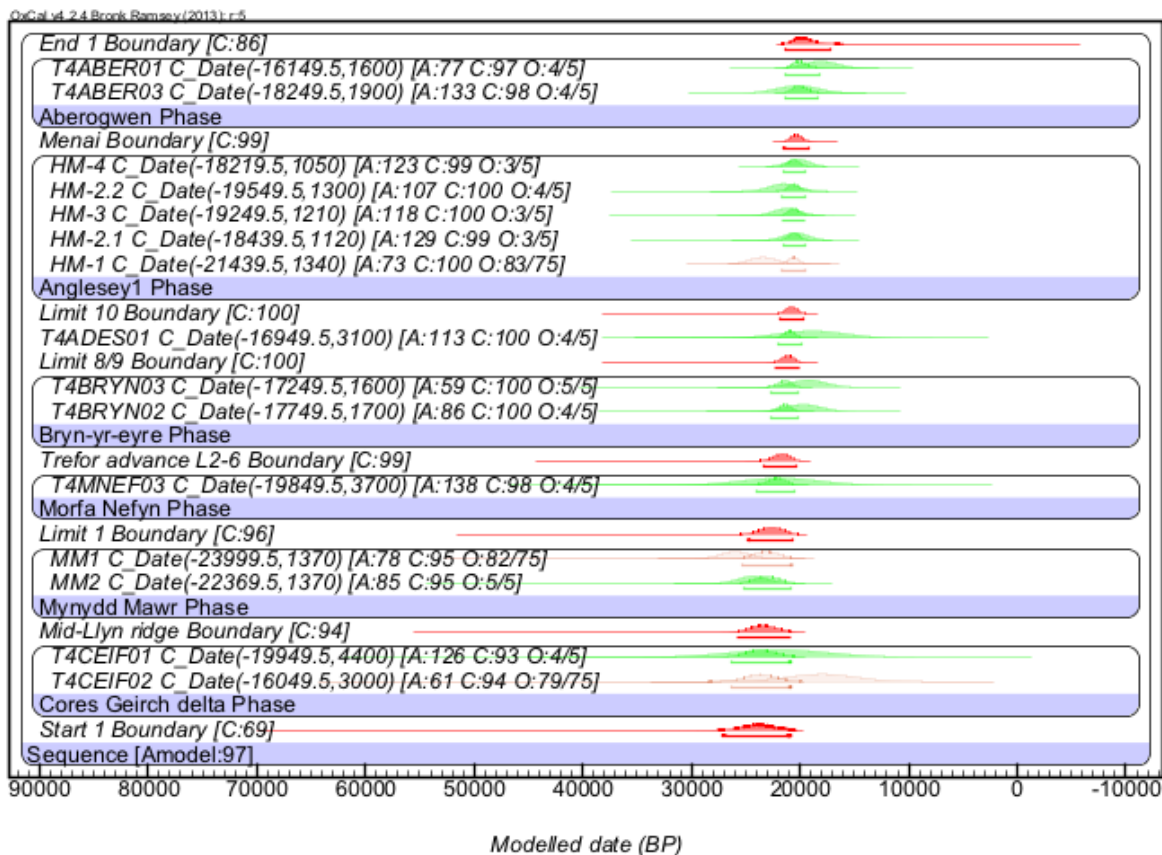


Fig. DR8. Bayesian model for the dating of ice retreat across the Llŷn Peninsula, and the model structure using OxCal keywords that define the relative order of events (Ramsey, 2009a). Each distribution (hollow) represents the relative probability of each age estimate with posterior density estimate (solid) generated by the modelling. Shown are conformable ages (green), outliers (orange) and modelled boundary ages (Red).

4. D_e VALUES DETERMINED FOR OSL DATING

Table DR5. D_e values from OSL dating of sample T4CEIF01.

D _e (Gy)	D _e Uncertainty (Gy)	Net T _n signal in response to 9.5 Gy (cts/0.1 s)
36.41	2.72	996
56.57	20.44	70
37.12	8.16	153
67.02	17.70	101
24.25	12.82	52
72.59	14.95	100
33.69	37.03	60
17.60	2.07	191
37.11	3.49	1238
42.77	9.53	748
23.23	7.79	56
78.79	8.31	1079
108.50	30.52	134
41.82	11.10	667
163.65	16.11	1141
185.40	22.29	384
40.46	10.87	102
80.72	40.02	142
106.06	18.15	113
236.77	44.80	56
47.60	11.66	88
44.93	13.67	625
142.92	17.23	183
126.50	24.24	527
118.17	21.18	88
22.59	6.23	72
133.08	151.59	52
113.09	10.89	159
17.96	5.53	47
120.19	13.28	353
124.43	18.45	2511
46.63	11.63	56
80.63	11.30	277
33.25	3.37	202
9.23	3.16	48
142.85	25.29	76
123.67	14.01	200
38.35	6.18	105
172.54	22.05	389
128.71	22.16	102
83.85	24.88	103
14.06	3.42	83
35.73	9.57	48
121.54	22.52	1235

147.08	14.24	370
94.41	7.78	377
127.22	18.15	159
152.26	18.98	1756
63.56	17.68	46
162.55	22.98	154
36.64	15.16	269
80.82	61.88	44
33.36	15.28	62
29.10	4.21	439

Table DR6. D_e values from OSL dating of sample T4CEIF02.

D_e (Gy)	D_e Uncertainty (Gy)	Net T_n signal in response to 9.5 Gy (cts/0.1 s)
37.83	8.44	89
149.96	51.87	80
22.36	2.97	292
31.90	3.93	327
34.03	11.41	336
55.16	3.50	1835
42.74	11.16	51
26.51	6.99	289
30.69	3.05	374
62.12	9.92	899
62.66	16.18	185
43.66	2.60	1010
30.32	2.14	11604
17.51	4.28	91
23.13	8.25	107
41.14	5.82	222
19.01	4.73	71
26.62	8.54	64
87.95	34.89	99
22.26	1.95	650
60.53	31.98	234
23.15	4.18	122
72.26	12.96	65
21.28	3.05	218
97.86	12.51	170
16.91	2.72	219
43.70	6.96	130
159.35	19.26	6860
23.58	9.47	90
37.20	5.92	413
79.84	7.25	301
75.42	33.16	66
71.22	13.13	84
46.61	2.62	3445
29.43	7.03	72

42.41	8.45	137
33.06	8.41	90
36.09	12.95	84
79.86	10.39	137
39.12	4.42	907
6.36	2.91	113
11.67	5.34	127
25.51	5.79	152
51.91	3.57	1712
93.71	19.54	126
11.56	4.48	67
14.29	2.02	525
43.25	6.88	139
25.76	6.05	71
56.28	17.06	55
79.88	18.15	45
25.43	5.77	48
13.83	1.86	149
91.91	8.87	167
112.85	13.15	154
104.03	26.58	118
25.50	5.04	100
115.47	16.68	96
36.38	16.01	136
39.88	3.79	317
28.15	8.66	52
102.05	14.57	213
124.42	26.79	69
22.28	6.74	88
83.52	21.13	730
136.53	14.96	1078
26.97	15.44	53

Table DR7. D_e values from OSL dating of sample T4MNEF03.

D_e (Gy)	D_e Uncertainty (Gy)	Net T_n signal in response to 13.0 Gy (cts/0.1 s)
119.55	13.24	316
33.52	10.67	40
24.79	6.56	75
102.79	30.83	52
41.26	6.70	138
36.36	11.81	41
53.93	13.23	81
99.60	22.88	43
104.11	30.92	603
24.10	4.56	124
166.43	30.75	95
28.05	17.87	94
148.84	30.28	61

44.14	4.93	259
25.25	5.41	91
67.82	13.56	89
73.47	12.16	359
22.40	7.41	66
48.12	10.70	81
33.25	6.60	60
154.64	31.95	128
191.29	42.76	44
85.33	24.86	133
98.35	23.08	57
50.03	9.89	94
135.17	26.81	292
19.91	2.50	452
39.75	10.26	51
21.14	2.29	280
74.84	16.19	93
79.75	6.62	148
31.32	4.52	48
37.36	12.64	50
17.38	2.88	140
108.62	67.14	56
80.76	98.40	42
114.07	40.91	63
59.22	9.50	160
188.76	14.23	577
176.81	97.08	177
137.36	36.60	108
70.96	27.54	70
86.16	33.75	151
30.55	3.79	177

Table DR8. D_e values from OSL dating of sample T4BRYN02.

D_e (Gy)	D_e Uncertainty (Gy)	Net T_n signal in response to 13.0 Gy (cts/0.1 s)
16.65	2.57	127
50.83	16.92	67
41.20	8.34	167
66.18	14.33	104
50.33	11.56	53
24.41	5.34	124
19.46	2.68	246
57.21	9.94	144
47.05	8.62	77
50.26	8.46	227
32.50	4.41	172
32.32	3.15	395
5.81	6.85	57
26.53	4.39	96

24.12	4.96	117
39.76	6.79	72
44.98	8.09	287
62.76	6.94	213
16.59	3.12	85
38.51	5.86	274
34.83	5.64	281
65.82	12.28	5302
18.94	2.35	240
36.87	4.67	209
12.58	3.75	40
47.29	12.02	49
25.93	4.14	163
10.08	4.26	122
45.79	4.32	447
29.22	3.59	227
32.54	9.70	37
74.10	12.64	103
27.82	14.71	54
32.82	19.14	70
40.15	8.99	126
77.59	5.74	3238
35.30	3.22	364
42.55	6.41	174
82.67	20.01	701
46.73	2.93	845
117.48	32.53	46
32.50	8.54	67
49.62	8.01	249
27.27	7.49	62
33.74	5.34	147
26.70	2.37	334
78.91	7.11	331
36.82	7.40	43
37.35	10.59	81
37.32	9.00	57
26.09	18.44	113
44.88	10.08	45
44.50	10.64	163
38.47	10.80	47
30.37	7.58	53

Table DR8. D_e values from OSL dating of sample T4BRYN03.

D_e (Gy)	D_e Uncertainty (Gy)	Net T_n signal in response to 13.0 Gy (cts/0.1 s)
41.15	13.77	121
26.85	6.13	52
37.67	17.33	67
47.37	4.53	393

79.68	22.77	39
42.72	3.25	1985
54.08	14.34	43
43.36	25.94	60
26.44	5.07	84
60.61	5.04	723
27.73	2.78	332
40.64	22.03	66
73.21	21.12	47
33.90	4.16	565
21.34	10.99	45
26.12	7.71	49
62.38	11.70	113
55.98	13.19	73
15.87	3.68	63
22.10	6.21	41
49.21	14.48	54
29.45	1.89	797
13.88	5.79	47
48.80	5.63	241
69.98	9.52	4886
58.73	10.34	91
63.21	13.87	358
40.64	5.60	249
31.40	11.59	39
54.70	4.85	483
19.51	6.55	42
42.32	10.08	141
29.57	6.26	115
4.27	5.99	50
82.03	36.25	165
33.54	11.89	109
49.86	11.22	56
61.02	19.47	43
58.68	10.50	522
44.60	28.72	75
68.62	16.01	41
44.75	5.60	485
48.71	5.44	229
93.89	25.23	90
201.48	35.19	206
37.24	3.96	376
36.01	7.49	58
30.10	7.26	64
19.84	5.17	141
36.98	3.49	1113
173.90	33.63	112
41.46	4.75	492
68.43	6.07	560

52.87	8.12	181
38.63	7.35	137
35.48	8.41	69
79.06	6.59	2184
57.32	6.68	2187
53.39	11.61	70
49.59	12.31	65
35.04	3.67	234
43.88	12.02	53
18.56	4.46	71
44.92	12.08	88
29.19	6.16	114
33.97	10.24	63
34.57	7.68	73
37.62	13.14	44
33.71	13.71	226

Table DR9. D_e values from OSL dating of sample T4ADES01.

D_e (Gy)	D_e Uncertainty (Gy)	Net T_n signal in response to 9.5 Gy (cts/0.1 s)
18.61	4.43	81
37.67	8.92	86
137.10	8.70	1011
31.59	8.54	62
121.87	22.87	164
56.57	13.16	50
62.28	7.18	713
188.71	16.38	3456
47.27	11.38	52
66.08	13.33	59
30.10	8.26	88
67.50	17.40	199
154.54	17.24	513
53.78	14.68	51
41.90	4.00	1285
175.53	81.97	63
72.38	16.75	52
106.17	9.63	1416
67.06	9.78	205
53.10	14.39	291
116.68	21.85	199
67.51	23.93	1903
39.37	10.71	123
86.46	8.87	529
68.39	13.48	60
45.32	10.80	66
84.12	17.36	136
157.84	12.08	324
85.84	8.81	250
54.19	12.39	52

46.52	6.78	234
102.51	37.13	392
47.58	15.75	72
52.04	5.78	268
88.40	18.74	632
102.83	36.35	72
45.72	47.55	117
44.38	6.97	151
57.80	3.82	608
166.02	42.26	456
118.35	10.64	8281
38.40	45.44	77
34.24	8.03	68
40.14	23.86	96
16.23	4.72	110
39.77	7.18	81
88.59	19.74	109
115.56	6.89	2262
37.68	8.91	55
60.68	14.86	48
123.16	17.43	1047
75.91	5.24	578
126.66	31.73	59
23.69	7.58	59
76.90	14.16	74
22.15	10.14	71
38.15	8.94	58
97.74	21.53	62
126.52	24.99	100
64.46	7.90	1121
38.43	3.19	500
64.45	10.73	184
65.97	7.69	322
61.51	12.63	815
43.00	4.95	424
27.52	4.65	196
39.08	11.96	92
53.92	7.70	136
103.20	25.40	209
89.18	25.15	226
43.74	8.02	114
80.11	5.53	9671
7.22	8.82	42
50.88	9.30	60
67.04	13.46	73
88.95	26.55	91
82.69	58.09	69

Table DR10. D_e values from OSL dating of sample T4ABER01.

D_e (Gy)	D_e Uncertainty (Gy)	Net T_n signal in response to 9.4 Gy (cts/0.1 s)
61.52	5.02	812
30.54	9.16	56
40.98	12.00	57
87.86	25.74	53
43.69	7.60	107
16.72	5.25	57
27.37	2.42	951
37.01	5.76	130
49.39	9.69	1005
33.49	11.58	177
63.40	4.29	6545
67.85	33.53	278
75.33	5.24	2487
48.78	5.80	132
31.49	5.81	81
45.91	7.31	244
89.57	28.04	48
46.74	12.01	86
55.47	13.33	195
35.10	9.29	67
39.22	4.03	415
31.76	2.92	445
98.30	6.97	4208
40.91	7.58	112
32.15	10.98	425
36.97	6.44	186
24.35	3.04	183
37.60	8.57	104
45.25	9.29	336
20.85	6.42	45
49.00	6.71	90
32.18	7.01	70
29.60	5.52	92

Table DR11. D_e values from OSL dating of sample T4ABER03.

D_e (Gy)	D_e Uncertainty (Gy)	Net T_n signal in response to 9.5 Gy (cts/0.1 s)
58.10	7.39	853
58.62	10.16	169
73.88	17.20	85
45.83	8.23	77
37.10	9.68	83
33.86	6.45	418
79.50	21.76	57
14.58	5.79	47

13.45	3.37	80
53.72	9.62	81
55.59	3.58	1213
50.71	9.09	113
100.33	44.11	105
34.27	11.54	50
78.74	22.84	48
102.47	44.71	51
82.10	31.81	413
54.14	8.16	178
46.57	12.33	92
14.99	1.77	766
13.98	5.86	51
41.65	7.40	120
57.82	13.50	61
41.75	5.80	150
98.17	26.49	50
76.16	21.81	65
34.78	3.16	279
86.98	12.64	171
90.25	12.40	161
62.74	19.53	56
96.02	74.14	521
57.99	17.16	50
72.94	20.57	675
24.70	7.03	148
88.22	21.68	1370
60.88	12.57	97
46.70	8.02	86
67.76	4.50	2060
96.38	19.83	200
15.74	4.68	52
60.97	9.76	718
106.42	25.07	256
28.22	6.01	82
60.35	14.48	623
50.30	13.88	60
82.50	11.16	521

5. BAYESIAN MODEL CODE INPUT INTO OXCAL

<pre>Options() { BCAD=FALSE; SD1=FALSE; SD2=FALSE; }; Plot() { Outlier_Model("General",T(5),U(0,4),"t"); Sequence()</pre>	<pre>{ Boundary("Start 1") { color="Red"; }; Phase("Cores Geirch delta") { C_Date("T4CEIF02", 18000, 3000) { Outlier("Test", 0.75); } } }</pre>
---	---

```

};
C_Date("T4CEIF01", 21900, 4400)
{
  color="Orange";
  Outlier("Test", 0.05);
};
};
Boundary("Mid-Llyn ridge")
{
  color="Red";
};
Phase("Mynedd Mawr")
{
  C_Date("MM2", 24320, 1370)
  {
    color="Blue";
    Outlier("Test", 0.05);
  };
  C_Date("MM1", 25950, 1370)
  {
    Outlier("Test", 0.75);
  };
};
Boundary("Limit 1")
{
  color="Red";
};
Phase("Morfa Nefyn")
{
  C_Date("T4MNEF03", 21800, 3700)
  {
    color="Orange";
    Outlier("Test", 0.05);
  };
};
Boundary("Trefor advance L2-6")
{
  color="Red";
};
Phase("Bryn-yr-Eyre")
{
  C_Date("T4BRYN02", 19700, 1700)
  {
    color="Orange";
    Outlier("Test", 0.05);
  };
  C_Date("T4BRYN03", 19200, 1600)
  {
    color="Orange";
    Outlier("Test", 0.05);
  };
};
Boundary("Limit 8/9")

```

```

{
  color="Red";
};
C_Date("T4ADES01", 18900, 3100)
{
  color="Orange";
  Outlier("Test", 0.05);
};
Boundary("Limit 10")
{
  color="Red";
};
Phase("Anglesey1")
{
  C_Date("HM-1", 23390, 1340)
  {
    Outlier("Test", 0.75);
  };
  C_Date("HM-2.1", 20390, 1120)
  {
    color="Blue";
    Outlier("Test", 0.05);
  };
  C_Date("HM-3", 21200, 1210)
  {
    color="Blue";
    Outlier("Test", 0.05);
  };
  C_Date("HM-2.2", 21500, 1300)
  {
    color="Blue";
    Outlier("Test", 0.05);
  };
  C_Date("HM-4", 20170, 1050)
  {
    color="Blue";
    Outlier("Test", 0.05);
  };
};
Boundary("Menai")
{
  color="Red";
};
Phase("Aberogwen")
{
  C_Date("T4ABER03", 20200, 1900)
  {
    color="Orange";
    Outlier("Test", 0.05);
  };
  C_Date("T4ABER01", 18100, 1600)
  {
    color="Orange";
  };
};

```

Outlier("Test", 0.05);		color="Red";
};		};
};		};
Boundary("End 1")		};
{		

REFERENCES

- Balco, G., Stone, J. O., Lifton, N. A., and Dunai, T. J., 2008, A complete and easily accessible means of calculating surface exposure ages or erosion rates from ^{10}Be and ^{26}Al measurements: *Quaternary Geochronology*, v. 3, no. 3, p. 174-195.
- Bøtter-Jensen, L., Andersen, C. E., Duller, G. A. T., and Murray, A. S., 2003, Developments in radiation, stimulation and observation facilities in luminescence measurements: *Radiation Measurements*, v. 37, no. 4-5, p. 535-541.
- Bronk Ramsey, C., 1995, Radiocarbon calibration and analysis of stratigraphy: the OxCal program: *Radiocarbon*, v. 37, no. 2, p. 425-430.
- Bronk Ramsey, C., 2008, Deposition models for chronological records: *Quaternary Science Reviews*, v. 27, no. 1-2, p. 42-60.
- Bronk Ramsey, C., 2009a, Bayesian analysis of radiocarbon dates: *Radiocarbon*, v. 51, no. 1, p. 337-360.
- Bronk Ramsey, C., 2009b, Dealing with outliers and offsets in radiocarbon dating: *Radiocarbon*, v. 51, no. 3, p. 1023-1045.
- Buck, C. E., Cavanagh, W. G., and Litton, C. D., 1996, Bayesian Approach to Interpreting Archaeological Data.
- Chiverrell, R. C., Thrasher, I. M., Thomas, G. S. P., Lang, A., Scourse, J. D., van Landeghem, K. J. J., McCarroll, D., Clark, C. D., Ó Cofaigh, C., Evans, D. J. A., and Ballantyne, C. K., 2013, Bayesian modelling the retreat of the Irish Sea Ice Stream: *Journal of Quaternary Science*, v. 28, no. 2, p. 200-209.
- Durcan, J. A., King, G. E., and Duller, G. A. T., 2015, DRAC: Dose Rate and Age Calculator for trapped charge dating: *Quaternary Geochronology*, v. 28, p. 54-61.
- Edge, M. J., Hart, J., and Pointon, K., 1990, The sequences at Aber Ogwen and Glan-y-mor-isaf, *in* Addison, K., Edge, M. J., and Watkins, R., eds., *The Quaternary of North Wales: Field Guide*: Coventry, Quaternary Research Association, p. 119-130.
- Eyles, N., and McCabe, A. M., 1989, The Late Devensian (<22,000 BP) Irish Sea Basin: The sedimentary record of a collapsed ice sheet margin: *Quaternary Science Reviews*, v. 8, no. 4, p. 307-351.
- Fabel, D., Ballantyne, C. K., and Xu, S., 2012, Trimlines, blockfields, mountain-top erratics and the vertical dimensions of the last British-Irish Ice Sheet in NW Scotland: *Quaternary Science Reviews*, v. 55, p. 91-102.
- Galbraith, R. F., and Laslett, G. M., 1993, Statistical models for mixed fission track ages: *Nuclear Tracks and Radiation Measurements*, v. 21, no. 4, p. 459-470.
- Galbraith, R. F., Roberts, R. G., Laslett, G. M., Yoshida, H., and Olley, J. M., 1999, Optical dating of single and multiple grains of quartz from Jinmium rock shelter, northern Australia: Part 1, experimental design and statistical models.: *Archaeometry*, v. 41, no. 2, p. 339-364.
- Guerin, G., Mercier, N., and Adamiec, G., 2011, Dose-rate conversion factors: update.: *Ancient TL*, v. 29, p. 5-8.
- Guerin, G., Mercier, N., Nathan, R., Adamiec, G., and Lefrais, Y., 2012, On the use of the infinite matrix assumption and associated concepts: A critical review: *Radiation Measurements*, v. 47, no. 9, p. 778-785.
- Lal, D., 1991, Cosmic ray labeling of erosion surfaces: in situ nuclide production rates and erosion models: *Earth and Planetary Science Letters*, v. 104, no. 2-4, p. 424-439.
- McCarroll, D., 2005, North-west Wales, *in* Lewis, C. A., and Richards, A. E., eds., *The glaciations of Wales and adjacent areas*: Bristol, Logaston Press, p. 27-40.
- McCarroll, D., Stone, J. O., Ballantyne, C. K., Scourse, J. D., Fifield, L. K., Evans, D. J. A., and Hiemstra, J. F., 2010, Exposure-age constraints on the extent, timing and rate of retreat of the last Irish Sea ice stream: *Quaternary Science Reviews*, v. 29, no. 15-16, p. 1844-1852.
- Murray, A. S., and Wintle, A. G., 2000, Luminescence dating of quartz using an improved single-aliquot regenerative-dose protocol: *Radiation Measurements*, v. 32, no. 1, p. 57-73.

- Prescott, J. R., and Hutton, J. T., 1994, Cosmic-Ray Contributions to Dose-Rates for Luminescence and ESR Dating - Large Depths and Long-Term Time Variations: *Radiation Measurements*, v. 23, no. 2-3, p. 497-500.
- Small, D., Clark, C. D., Chiverrell, R. C., Smedley, R. K., Bateman, M. D., Duller, G. A. T., Ely, J. C., Fabel, D., Medialdea, A., and Moreton, S. G., 2017, Devising quality assurance procedures for assessment of legacy geochronological data relating to deglaciation of the last British-Irish Ice Sheet: *Earth-Science Reviews*, v. 164, p. 232-250.
- Stone, J. O., 2000, Air pressure and cosmogenic isotope production: *Journal of Geophysical Research: Solid Earth*, v. 105, no. B10, p. 23753-23759.
- Thomas, G. S. P., and Chiverrell, R. C., 2007, Structural and depositional evidence for repeated ice-marginal oscillation along the eastern margin of the Late Devensian Irish Sea Ice Stream: *Quaternary Science Reviews*, v. 26, no. 19-21, p. 2375-2405.
- Thomas, G. S. P., Connaughton, M., and Dackombe, R. V., 1985, Facies variation in a Late Pleistocene supraglacial outwash sandur from the Isle of Man: *Geological Journal*, v. 20, no. 3, p. 193-213.
- Thomsen, K. J., Murray, A. S., and Bøtter-Jensen, L., 2005, Sources of variability in OSL dose measurements using single grains of quartz: *Radiation Measurements*, v. 39, no. 1, p. 47-61.
- Thrasher, I. M., Mauz, B., Chiverrell, R. C., Lang, A., and Thomas, G. S. P., 2009, Testing an approach to OSL dating of Late Devensian glaciofluvial sediments of the British Isles: *Journal of Quaternary Science*, v. 24, no. 7, p. 785-801.